

PHYSICAL REVIEW B

CONDENSED MATTER AND MATERIALS PHYSICS

THIRD SERIES, VOLUME 60, NUMBER 18

1 NOVEMBER 1999-II

RAPID COMMUNICATIONS

Rapid Communications are intended for the accelerated publication of important new results and are therefore given priority treatment both in the editorial office and in production. A Rapid Communication in Physical Review B may be no longer than four printed pages and must be accompanied by an abstract. Page proofs are sent to authors.

Martensitic textures: Multiscale consequences of elastic compatibility

S. R. Shenoy

Abdus Salam International Centre for Theoretical Physics, Trieste 34100, Italy

T. Lookman, A. Saxena, and A. R. Bishop

Theoretical Division, Los Alamos National Laboratory, Los Alamos, New Mexico 87545

(Received 10 August 1999)

We show that a free energy entirely in the order-parameter strain variable(s), rather than the displacement field, provides a unified understanding of martensitic textures. We use compatibility equations, linking the strain tensor components in the bulk and at interfaces, that induce anisotropic order-parameter strain interactions. These two long-range bulk/interface potentials, together with local compositional fluctuations, drive the formation of global elastic textures. Relaxational simulations show the spontaneous formation (and evolution under stress/temperature quenches) of equal width parallel twins, branched twins, and tweed, including characteristic scaling of twin width with twin length. [S0163-1829(99)51442-2]

Martensitic structural transitions,¹ especially those with unit cells related by continuous deformations, exhibit a rich variety of temperature/stress induced microtextures.²⁻⁴ For example, alloys such as FePd and NiTi, that show the shape memory effect,⁵ transform on cooling from a higher symmetry phase (“austenite”), through nanometer-scale “tweed” textures, to equal-width mesoscale “twins” below the (“martensite”) transition temperature T_0 . One (or more) of the gradients of the atomic displacement vector, or *strain tensor* component(s), acts as the natural order parameter (OP) for these unit-cell transformations, observable by neutron-scattering or high-resolution electron microscopy (HREM) methods.²⁻⁴ However, a displacement-field description (that enforces elastic continuity requirements) has been generally used. For example, the experimentally observed square-root dependence of martensitic twin width on twin length has been understood as a consequence of the austenite region fringing fields,⁶ but only by going back to displacement vectors, matched at the interface. Similarly, numerical simulations of tweed textures⁷ have used the displacement vector as the fluctuating variable. Other treatments, with morphological profiles as the order parameter,^{8,9} also rely on arguments based on local displacement vectors and do not explicitly consider an interface with austenite. We show, however, that bulk/interface elastic compatibility constraints

can be expressed in terms of long-range anisotropic strain forces (that are masked in a conventional displacement-field treatment). A consistent Ginzburg-Landau (GL) understanding of martensitic textures in terms of the OP strain alone, and involving long-range OP strain-strain forces, is possible. This could have a wider impact on modeling microstructures in other materials such as proper/improper ferroelectrics, magnetoelastics, and shape memory alloys.

The OP is one or more components of a strain tensor $\varepsilon_{\mu\nu}(\mu, \nu = x, y, z)$, not a true scalar. For simplicity, we consider a two-dimensional (2D) square-to-rectangle transformation,^{6,7,10,11} with a rectangular or deviatoric strain as an OP. The non-OP strain components are implicit functions of the OP, through a compatibility (differential) equation.¹² Thus the apparently innocuous GL terms harmonic in the non-OP components are crucial: they generate two effective long-range anisotropic OP potentials, from the bulk and from the austenite-martensite interface, or “habit plane.” Their combined action plays a decisive role in the energetic competition between various OP textures, e.g., for temperatures $T < T_0$, oriented, equal-width twins are favored, emerging into the bulk from the habit plane. They also affect global tweed formation for $T > T_0$, induced in our GL model by alloy compositional fluctuations, that act as local internal microstresses. Simple and local external stresses, acting

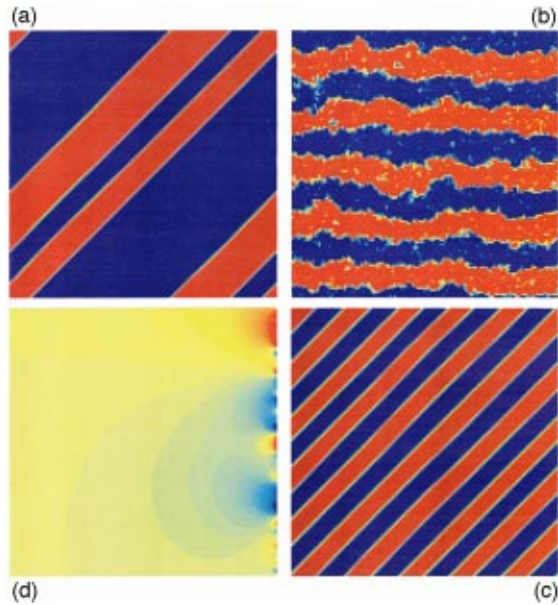


FIG. 1. (Color) Clockwise from upper left: (a) Oriented $\pi/4$ parallel structure obtained from bulk compatibility potential only. (b) Unoriented “twins” obtained from surface compatibility potential only. (c) Oriented twins with both bulk and surface compatibility present. (d) The corresponding decaying elastic fringing field in the austenite.

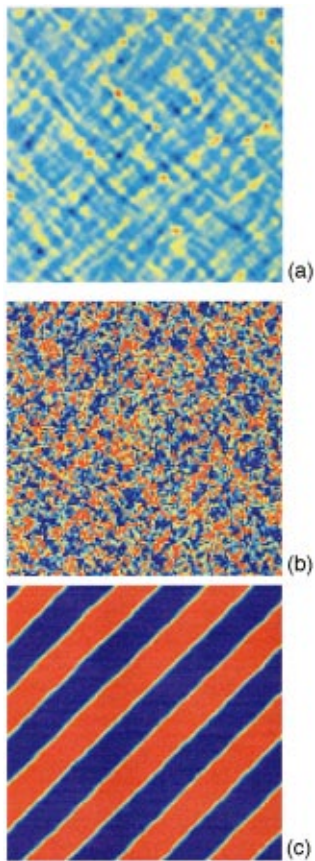


FIG. 3. (Color) From top: Spontaneous formation of states on cooling through a transition value of $\tau=0.52$ (reduced by spatial variations from the mean field $\tau=1.0$). (a) Austenite at $\tau=1.0$, (b) tweed at $\tau=0.65$, and (c) twins at $\tau=0.4$.

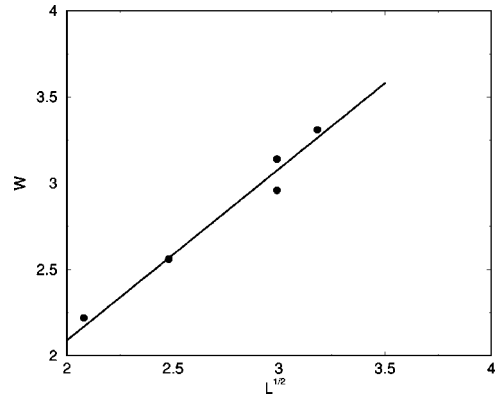


FIG. 2. Plot of $\ln(W/W_0)$ versus $\ln(L/L_0)^{1/2}$, where $W, L(W_0, L_0)$ are the twin width and twin length (parameter dependent scale factors).

through compatibility-induced long-range potentials, can generate complex and extended multiscale structures, through adaptive elastic screening.

Model. Our GL model in 2D consists of (i) a triple-well potential F_0 , as is usual for first-order transitions, in the

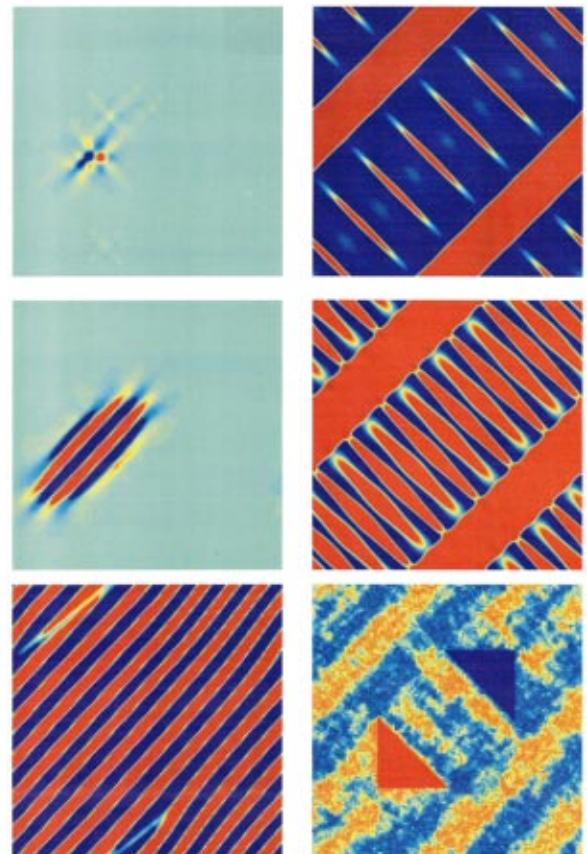


FIG. 4. (Color) Effect of a temperature quench and stress, on the (suitably seeded) states of Fig. 3: (a) left column, from top down, a time sequence showing how a “temperature quench” of austenite to $\tau=0.3$ results in nucleation and growth of twinned martensite. (b) Right column, top and middle, a time sequence under external uniform stress $P = -1.8$ for $\tau=0.45$ twins, inducing hierarchy and branching of twins. (c) Right column, bottom, embossing tweed with a local stress (with $P = \pm 50$ inside triangles only). A global microstructure develops, in response.

deviatoric strain OP [$\epsilon = (1/\sqrt{2})(\epsilon_{xx} - \epsilon_{yy})$]; (ii) a harmonic (linear) elastic energy cost F_{cs} due to the compressional [$e_1 = (1/\sqrt{2})(\epsilon_{xx} + \epsilon_{yy})$] and shear ($e_2 = \epsilon_{xy}$) strain that implicitly depend on the OP through compatibility; (iii) the coupling of strain(s) to an external or internal (defect, dislocation) stress; (iv) second and fourth-order strain gradient terms F_{grad} that induce multiscale competition; and (v) symmetry-allowed couplings F_{compos} of the (scalar) compositional fluctuations $\tilde{\eta}(r)$ to the OP and its derivatives.

The (dimensionless) elastic energy in 2D is given with $\epsilon = \epsilon(r)$, by

$$F = F_0(\epsilon) + F_{grad}(\nabla\epsilon) + F_{cs}(e_1, e_2) + F_{compos}(\epsilon); \quad (1)$$

$$F_0(\epsilon) = \sum_r [(\tau - 1)\epsilon^2 + \epsilon^2(\epsilon^2 - 1)^2 - P(r)\epsilon(r)], \quad (2a)$$

$$F_{grad}(\nabla\epsilon) = \sum_r [(a/4)(\nabla\epsilon)^2 + (b/8)(\nabla^2\epsilon)^2], \quad (2b)$$

$$F_{cs}(e_1, e_2) = \frac{1}{2} \sum_r [A_1 e_1^2 + A_2 e_2^2], \quad (2c)$$

$$F_{compos}(\tilde{\eta}, \epsilon, \nabla\tilde{\eta}) = \sum_r [A^{(T)}\tilde{\eta}(r)\epsilon^2 - A^{(P)}\epsilon(r)\tilde{P}(r)]. \quad (2d)$$

Here $P(r)$ and $\tau = (T - T_c)/(T_0 - T_c)$ are dimensionless external deviatoric stress and scaled temperature, respectively, with T_c the temperature at which the shear modulus would soften completely. For a specific material the coefficients can be determined from the measured phonon-dispersion data.¹³ The coefficients A_1 , A_2 , and $A^{(T)}, A^{(P)}$ are elastic constants for compression, shear, and compositional fluctuations, respectively. We will neglect the ‘‘transition temperature fluctuation’’ term,⁷ that is, we set $A^{(T)} = 0$. In Eq. (2d), $\tilde{P}(r) \equiv (\nabla_x^2 - \nabla_y^2)\tilde{\eta}(r)$, so the term retained describes a ‘‘compositional stress fluctuation’’ model. With a partial integration, treating $\tilde{\eta}(r)$ as a Gaussian random variable, both annealed and quenched averages yield $F_{compos}(\epsilon, \nabla\tilde{\eta}) \rightarrow F_{compos}(\nabla\epsilon) = -\alpha(T)\sum_r [(\nabla_x^2 - \nabla_y^2)\epsilon]^2$, with the coefficient α acquiring a temperature-dependence, in the quenched case, remaining positive above T_0 .¹⁴ As justified below, we will use this (averaged) term, that favors nucleation of tweed, in our simulations.

The dynamics of the continuous OP is assumed to be of the time dependent GL or relaxational type,

$$\dot{\epsilon}(r) = -\delta F(\epsilon(r), e_1[\epsilon(r)], e_2[\epsilon(r)])/\delta\epsilon(r), \quad (3)$$

where time t is scaled with a characteristic relaxation rate. The compression-shear (CS) strains $e_1(r)$ and $e_2(r)$ are written in terms of the order parameter $\epsilon(r)$ by solving the elastic compatibility (differential) equation.

Theoretical analysis. The St. Venant compatibility equation satisfied by the symmetric tensor ϵ is $\nabla \times (\nabla \times \epsilon) = 0$. The analysis with six strain tensor components in 3D can be carried out,¹⁵ but for simplicity, we confine our discussion to 2D with a compatibility constraint, satisfied at all times, that in the absence of defects is,^{7,16}

$$\nabla^2 e_1(r) - \sqrt{8}\nabla_x \nabla_y e_2(r) = (\nabla_x^2 - \nabla_y^2)\epsilon(r). \quad (4)$$

For (Fourier-expandable) strains $\epsilon(r)$ in the bulk, one obtains via the Lagrangian multiplier formalism⁷ that

$e_1(\vec{k}), e_2(\vec{k})$ are proportional to $\epsilon(\vec{k})$, with \vec{k} -dependent coefficients. An OP strain-strain potential $F_{cs}(\epsilon) = F_{cs}^{(bulk)} + F_{cs}^{(surface)}$ replaces (2c), where $F_{cs}^{(bulk)} = \sum_k U^{(bulk)}(\vec{k})|\epsilon(\vec{k})|^2$ and

$$U^{(bulk)}(\vec{k}) = \frac{(2A_1/A_2)[(k_x^2 - k_y^2)/k^2]^2}{1 + (8A_1/A_2)k_x^2 k_y^2/k^4}. \quad (5)$$

The real-space asymptotic analytic form is¹⁴ $U^{(bulk)}(\vec{r} - \vec{r}') \sim \cos[4(\theta - \theta')]/(\vec{r} - \vec{r}')^2$, with the $\sim 1/r^2$ falloff arising from 2D phase space. Thus correlations between $\epsilon(r) = +|\epsilon|$ and $\epsilon(r') = -|\epsilon|$ such as occur in tweed/twins, will be favored along the diagonals, at $\theta = \pm \pi/4$ orientations.

At a habit plane along $x=0$, for example, the decaying strain contributions require a mixed Fourier ($e^{ik_y y}$)–Laplace ($e^{-K_x |x|}$) expansion. The total e_1 , e_2 , and ϵ strains must satisfy continuity and compatibility across the habit plane. The mutually perpendicular decay and oscillation wave vectors K_x and k_y , respectively, are thereby linked: $K_x = K_x(|k_y|)$ (and in fact, K_x scales as $|k_y|$). Since strains in the $x < 0$ austenite *must* decay, $K_x \neq 0$, there must be a $k_y \neq 0$ ripple, i.e., twinning, in the $x > 0$ martensite (Fig. 1, below). The surface contribution to F_{cs} from $x < 0$ is then

$$F_{cs}^{(surface)} = (A_2/2) \sum_k |\tilde{\epsilon}(K_x(\vec{k}), k_y)|^2/|k_y|. \quad (6)$$

Note that $k_y = 0$ uniform phases are disfavored. In a generalization¹⁴ of the bulk case,⁷ all other (e_1, e_2) strains on both sides of the habit plane are proportional to the bulk OP strain $\epsilon(\vec{k})$, with \vec{k} -dependent coefficients. In particular, $\tilde{\epsilon}$, the OP strain for $x < 0$ on the austenite side, has a Fourier-Laplace coefficient $\tilde{\epsilon}(K_x(\vec{k}), k_y) = (1/2)[1 + iI(\vec{k})/J]\epsilon(\vec{k})$, where the orientation factor $I(\vec{k})$ and the coefficient $J(K_x)$ are known functions, and the decay wave vector K_x is determined by the compatibility condition (4), applied across the habit plane. In terms of a displacement field $\vec{u}(\vec{k}) \sim \epsilon(\vec{k})/|k_y|$, Eq. (6) is essentially the elastic fringing field found earlier,⁶ but here obtained directly from compatibility, and through a strain-only argument. To investigate twins, tweed, and other textures, one can do theoretical/simulation modeling in terms of the bulk OP strain alone, with the ‘‘displacement-field bookkeeping’’ done automatically in the bulk and at interfaces, through the corresponding compatibility-induced potentials.

In the present model, OP tweed is induced by the local stress term $F_{compos} \sim -\tilde{P}(r)\epsilon(r)$ of Eq. (2d) arising from compositional fluctuations, plus the long-range potential $F_{cs}^{(bulk)}(\epsilon)$ of Eq. (5). There are at least three other models for tweed in the literature: (a) a static model based on disorder-induced T_0 fluctuations, with tweed as random local metastable minima in a quenched spin-glass-like picture;⁷ (b) a kinetic nucleation model based on point defect-induced long-range strains⁸ with tweed as a saddle-point transient microstructure accessed by a temperature quench; and (c) a model based on an ordering interaction that is mediated by elastic relaxation in the material.⁹ We found in simulations¹⁴ that a local stress, nonzero $\tilde{\eta}(r) = \pm|\tilde{\eta}|$ at only two sites in Eq. (2d), induced tweedlike OP textures even at far-off sites. The physical reason is that the F_{cs} long-range po-

tential, representing energy costs from nonzero $e_1(r)$ and $e_2(r)$, induces “screening,” or a spontaneous generation of energy-lowering higher elastic multipoles, i.e., tweedlike textures. (The response is even more pronounced, with some finite disorder.) This compatibility-induced global texturing driven by local compositional stress justifies the use of the averaged effective $F_{compos} \sim -[(\nabla_x^2 - \nabla_y^2)\epsilon(r)]^2$ in the simulations presented here. It clearly favors the crisscrossing of domain walls oriented along the diagonals, i.e., tends to induce tweed formation, with $e_1, e_2 \neq 0$ by Eq. (4). We now show that a rich range of textures, similar to experiment, is supported by the model.

Texture simulations. We take random initial conditions, a 256×256 lattice, and periodic boundary conditions in both x and y directions to obtain relaxed textures $\epsilon(r)$. The actual finite-system strain components, including those in the surrounding austenite, are derived from the bulk $\epsilon(\vec{k})$. Full Langevin dynamics would involve a random force at every instant, to simulate the temperature: here we have a less time-consuming relaxational dynamics, with “Langevin bursts” at (small) temperature changes, to explore competing structures. We outline the simulation results obtained with the following typical (scaled) parameters for a representative material, $\text{Fe}_{0.7}\text{Pd}_{0.3}$: $A_1=1$, $A_2=2$, $a=4$, $T_0=1.2$, $T_c=0.52$, and $b=0.05$. The red/blue/green color shades represent ϵ positive/negative/zero OP strain values, respectively.

In Fig. 1(a) we show the formation of low-temperature $T < T_0$ parallel-domain structures with only bulk compatibility included. Note that the structures have the proper 45° orientation (as in Ref. 7) but are not true twins: there is no well defined width scale.⁶ In Fig. 1(b) we depict horizontal twinlike structures with only the surface compatibility term included. Now there is a dominant length scale (twin width) in the system but the “twins” have rough interfaces and are not properly oriented. When both bulk and surface compatibility terms are included we obtain equally spaced, parallel, and properly oriented twins, as shown in Fig. 1(c). The corresponding derived (deviatoric) OP strain field $\tilde{\epsilon}(r)$ in the austenite⁶ falls off as “decaying twins” away from the habit plane, as depicted in Fig. 1(d). With variation in system size L , the twin width scales as $W \sim \sqrt{L}$ (see Fig. 2). Thus our model clearly captures the essential physics of twinning in these materials.¹⁷

Figure 3 shows the transformation of textures under gradual cooling, from high-temperature austenite, through (“configurational glass”) tweed above the transition, to martensitic twins below the transition. Figure 4 depicts the evolution of these (suitably seeded) austenite/tweed/twinned martensite states, under temperature quenches and external stress. Figure 4(a) shows how $T \gg T_0$ austenite such as in Fig. 3(a) (with a small thermal zero-average OP fluctuation), evolves to twinned martensite, under a temperature quench to $T < T_0$. Note the lenticular twin shapes, surrounding elas-

tic field, and the “skew-varicose” interface instability just before the twinning is complete. This instability is also observed in granular media and convective rolls in fluids.¹⁸ The CS strains, derivable from the bulk OP strain through compatibility, are not shown. For $T < T_0$, they are expelled to the interface when equilibrium (diagonal) OP twins finally emerge. By contrast, the $T > T_0$ OP tweed, such as in Fig. 3(b), shows e_1 and e_2 strains in the bulk, localized at the domain-wall crossing points and corners. This is reminiscent of type-II superconductors, with $T_0 \sim T_{c1}$, and with twin (tweed) textures acting like Meissner (vortex) phases, expelling (allowing localized) shear strains that are like transverse vector potentials.

Branched twins^{16,19} have been observed under dynamic biaxial loading in the shape memory alloy CuAlNi .²⁰ Figure 4(b) shows how twins can divide under uniform external stress. The growth of (at least two generations of) hierarchical twinning is shown. A new generation of twins nucleates when the elastic strain between two preexisting twins exceeds a critical value. Branched twinlike structures may be seen where the fine twins meet the coarser ones.

The metastable tweed microstructure shows an interesting, anisotropic long-range strain response to “embossing” by an applied local stress. A deviatoric strain pattern (two $\pm|e|$ triangular regions) applied to the tweed of Fig. 3(b), produces the globally modified and multiscale, characteristic microstructure depicted in Fig. 4(c). (Tweed and these externally imposed textures are both the result of compatibility-related response to stresses: the first microscopic, random, and internal; the second macroscopic, systematic, and external.) This raises the intriguing possibility¹¹ of encoding large-scale stress patterns in multiscale hierarchies of domain-wall strain textures, that act as elastic holograms for the erasure/recovery steps of a shape memory cycle. Further, with simple couplings to charge and spin fields, the long-range elastic potentials provide a generic strain-mediated mechanism for “stripes” in cuprates and manganates. Quantitative diagnostics for multiscale textures include the multi-peaked, anisotropic structure factor $|\epsilon(\vec{k})|^2$.

In conclusion, the tensorial character of the martensite order parameter implies that other non-OP strains are coupled to its variations, through elastic compatibility, generating a Ginzburg-Landau model in terms of the OP strain alone. At low temperatures, the compatibility-induced anisotropic long-range potential in the bulk and at interfaces, induces equal-width and oriented twins. At higher temperatures, in conjunction with compositional stress, it induces tweed textures. Simple local external stresses can produce complex nonlocal strains, in elastic response. Thus, the rich variety of observed multiscale martensitic textures can be understood as a consequence of elastic compatibility.

We wish to thank R. C. Albers, G. R. Barsch, W. C. Kerr, J. A. Krumhansl, D. Sherrington, and P. J. Swart for insightful discussions. This work was supported in part by the U.S. Department of Energy under Contract No. W-Z405-ENG-36.

¹Z. Nishiyama, *Martensitic Transformations* (Academic, New York, 1978).

²L.E. Tanner *et al.*, *J. Phys. (Paris), Colloq.* **43**, C4-169 (1982).

³R. Oshima *et al.*, *Metall. Trans. A* **19**, 803 (1988).

⁴M. Sugiyama, Ph.D. thesis, Osaka University, 1985.

⁵*Shape Memory Effect in Alloys*, edited by J. Perkins (Plenum, New York, 1975).

⁶G.R. Barsch *et al.*, *Phys. Rev. Lett.* **59**, 1251 (1987); B. Horovitz

- et al.*, Phys. Rev. B **43**, 1021 (1991).
- ⁷S. Kartha *et al.*, Phys. Rev. Lett. **67**, 3630 (1991); S. Kartha *et al.*, Phys. Rev. B **52**, 803 (1995).
- ⁸S. Semenovskaya and A.G. Khachaturyan, Phys. Rev. Lett. **67**, 2223 (1991); Physica D **66**, 205 (1993); for 3D, see Y. Wang and A.G. Khachaturyan, Acta Mater. **45**, 759 (1997).
- ⁹A.M. Bratkovsky *et al.*, Phase Transit. **52**, 77 (1994); **55**, 79 (1995).
- ¹⁰A.E. Jacobs, Phys. Rev. B **31**, 5984 (1985); **46**, 8080 (1992); **52**, 6327 (1995).
- ¹¹A. Saxena *et al.*, Physica A **239**, 18 (1997); J. Phys. IV **5**, 125 (1995).
- ¹²D. S. Chandrasekharaiah and L. Debnath, *Continuum Mechanics* (Academic, San Diego, 1994), p. 218.
- ¹³G. R. Barsch and J. A. Krumhansl, in *Proceedings of the International Conference on Martensitic Transformations* (ICOMAT-92), edited by C. M. Wayman and J. Perkins (Monterey Inst. Adv. Studies, Monterey, 1993), p. 53.
- ¹⁴S. R. Shenoy *et al.* (unpublished).
- ¹⁵T. Lookman *et al.* (unpublished).
- ¹⁶W. C. Kerr *et al.*, Phase Transit. **69**, 247 (1999).
- ¹⁷Other materials like fcc/bcc steels, can access bcc twin phases through a temperature quench, with vacancy fields at moving interfaces. See, e.g., M. Rao, S. Sengupta, and H.K. Sahu, Phys. Rev. Lett. **75**, 2164 (1995).
- ¹⁸J.R. DeBruyn *et al.*, Phys. Rev. Lett. **81**, 1421 (1998).
- ¹⁹R.V. Kohn and S. Müller, Philos. Mag. A **66**, 697 (1992).
- ²⁰C. Chu, Ph.D. thesis, University of Minnesota, 1993; R. Abeyaratne *et al.*, Philos. Mag. A **73**, 457 (1996).